IEEE Photonics Journal
An IEEE Photonics Society Publication

Open Access

Numerical Analysis of Magnetic Plasmonic Resonance Modes in Three-Dimension Split Ring Resonator Metamaterials

Volume 11, Number 4, August 2019

Wei Wang
Feng-Ping Yan
Si-Yu Tan
Hai-Su Li
Xue-Mei Du
Hong Zhou
Ya-Fei Hou, ***Senior Member, IEEE***

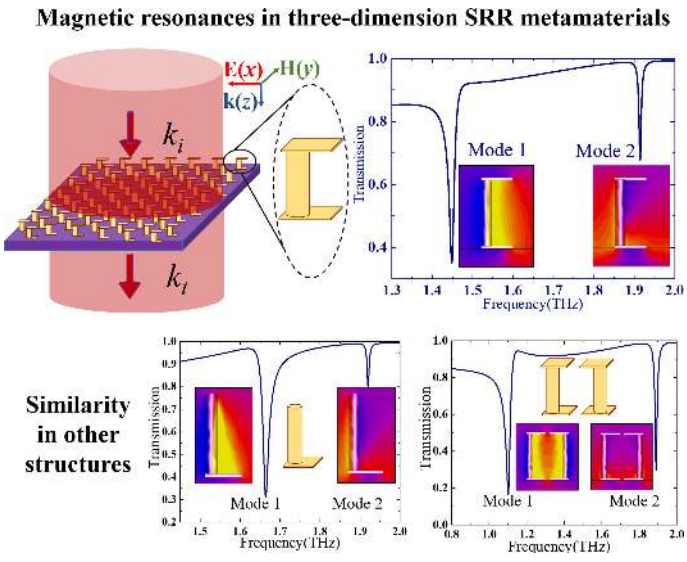

DOI: 10.1109/JPHOT.2019.2917539
1943-0655

Numerical Analysis of Magnetic Plasmonic Resonance Modes in Three-Dimension Split Ring Resonator Metamaterials

Wei Wang,[1] **Feng-Ping Yan**,[1] **Si-Yu Tan**,[1,2] **Hai-Su Li**,[1] **Xue-Mei Du**,[1] **Hong Zhou**,[3] **and Ya-Fei Hou**,[4] ***Senior Member, IEEE***

[1]Key Laboratory of All Optical Network and Advanced Telecommunication of EMC, Institute of Lightwave Technology, Beijing Jiaotong University, Beijing 100044, China
[2]Zhengzhou Xinda Institute of Advanced Technology, Zhengzhou 450001, China
[3]Department of Electronics, Information and Communication Engineering, Osaka Institute of Technology, Asahi-ku 535-8585, Japan
[4]Graduate School of Natural Science and Technology, Okayama University, Kita Ward 700-8530, Japan

DOI:10.1109/JPHOT.2019.2917539

Manuscript received March 11, 2019; revised May 9, 2019; accepted May 14, 2019. Date of publication May 17, 2019; date of current version July 26, 2019. This work was supported in part by the National Natural Science Foundation of China (NSFC) under Grants 61620106014, 61827818, and 61805010, and in part by the Beijing Natural Science Foundation under Grant 4192048. Corresponding author: Feng-ping Yan (e-mail: fpyan@bjtu.edu.cn).

Abstract: Magnetic resonators based on metamaterials are valuable for numerous applications including perfect absorber, sensing and medical imaging. However, due to the existence of the difficulty in magnetic excitation in planar metasurface, the study of magnetic metamaterial resonators is less reported, particularly in contrast to the electrical resonators. In this paper, the three-dimensional split ring resonator (SRR) metamaterials featuring dual-band magnetic plasmonic resonance modes are proposed and numerically analyzed. We calculate the electromagnetic field distributions of the three-dimensional metamaterials at the resonant frequencies to elucidate the resonant characteristics of the dual modes (fundamental LC mode and high-order magnetic plasmonic resonance mode). The influences of geometric parameters of the constituent meta-atoms on the resonance frequencies of the two resonance modes are analyzed by numerical calculations. The results show that the resonance frequency of the high-order magnetic resonance mode is nearly independent of the standing columns of the metamaterials owing to the special resonant characteristic of the high-order mode. Benefiting from the independence, the frequency interval between the dual modes can be customized by adjusting the dimensions of the column. In addition, by tuning the dimension of the columns, the quality factors of the resonances can reach the highest value of 176 for LC mode and 270 for the high-order mode, respectively. In light of practical application, we evaluate refractive index sensing performance of the proposed metamaterials, the maximum sensitivity can reach 474 GHz/RIU for LC mode and 446 GHz/RIU for high-order resonance, respectively. We also explore the universality of the special resonant characteristic of the high-order mode in other similar three-dimension SRR metamaterials, which shows all of these three-dimension magnetic plasmonic metamaterials provide potential platforms for multiband magnetic metamaterial applications.

Index Terms: Metamaterials, magnetic plasmon resonance.

1. Introduction

Metamaterials, consisting of sub-wavelength meta-atoms, can exhibit a variety of naturally unavailable attributes and unconventional phenomena, such as high or negative refractive index [1]–[3], sub-wavelength resolution imaging [2] and inverse Doppler effect [4]. By flexibly and intentionally engineering the structures, dimensions and arrangement of the constituent meta-atoms, metamaterials are able to functionalize as efficient electromagnetic (EM) devices to control the amplitude and phase of EM wave [5]–[10]. These controllable behaviors benefit mainly from the resonant characteristic inherent in various metamaterials [11]–[16]. In other words, by customizing the resonant behavior of metamaterials on purpose, the scattering, absorptive and dispersive response of metamaterials to incidence EM wave can be manipulated freely. Given this, scientific researchers pay high attention to designing and tuning various resonances in metamaterials in these years [13]–[15], [17]. However, most of the research works revolve around the electric excitation resonances while the counterpart, the magnetic excitations of resonances, are just explored to a limited extent.

It is well-established that magnetic resonances in metamaterials can be excited by either electric coupling or magnetic coupling. The electric coupling, mainly realized in the planar metamaterials, can only excite magnetic moment with the direction normal to the magnetic component of the incident wave [13], [18]. In this case, this orthogonal relation makes the resulted magnetic response to the incident wave is too weak to be utilized in practical application. As for the magnetic coupling, the magnetic response can be easily realized at microwave frequencies, however, when the response frequency reaches THz or even higher, the magnetic excitation in the planar metamaterials becomes challenging in the common case of normal incidence. To meet this challenge, the three-dimension split ring resonators (SRR) metamaterials, which are capable of being excited by a normally incidence THz radiation, were proposed [19]–[22]. Based on the three-dimension SRR structure, a wealth of intriguing functionalities have been reported in recent years, for example, tunable devices [23], beam steering [24], quantum phenomenon-like response [25], [26], high-quality toroidal resonance excitation [27], plasmon coupling [28] and sensors [29]–[31]. Beyond that, magnetic metamaterials which have stimulated a wide varieties of applications of significant importance including magnetically controllable physics [32]–[34], nonlinear effect [35], magnetoelastic metamaterials [36], optical activity [37], magnetic surface plasmon [38], [39], nonreciprocal waveguiding [40] and absorption [41] and medical imaging [42], are as useful as the electric counterpart and worth in-depth study.

To enrich the research of magnetic resonators based on metamaterials, we propose a standup SRR metamaterials. In this paper, we first illustrate this three-dimension SRR metamaterials consisting of top and bottom metal plates separated by metal columns, which features two sharp magnetic plasmonic resonances at terahertz band under normal incidence. After that, the EM filed intensity distributions of the proposed metamaterials at the resonant frequencies are analyzed numerically to unveil the physical content of the resonances. Then the impact of the geometric parameters of the metamaterials on the spectral response of the dual-band resonances, i.e., fundamental LC resonance and the high-order magnetic plasmonic resonance (HMPR), are discussed by tuning the dimensions of the proposed metamaterials. Finally, we explore the promising sensing prospective of the proposed metamaterials and also present that similar HMPR mode also exists in other similar three-dimension SRR metamaterials.

2. Metamaterials Design and Analysis

2.1 Structural Design

Fig. 1(a) presents the schematic diagram of our proposed metamaterials under normal incidence where the input and output EM wave vectors are indicated as k_i and k_t, respectively. In our configuration, the THz wave illuminates the metamaterials sample vertically from the top along z direction. The magnetic field component passes through the three-dimension SRRs perpendicularly along y direction while the electric field component is along x direction parallel to the long side of the metal

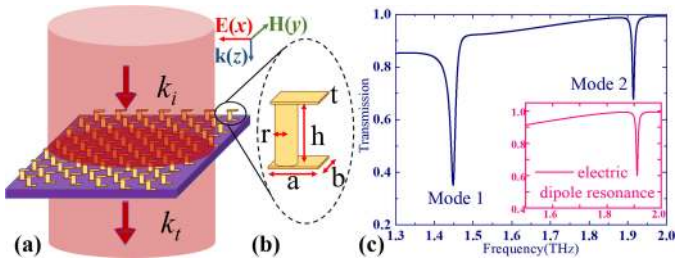

Fig. 1. (a) 3D schematic of the proposed metamaterials and the EM field polarizations. (b) A SRR unit cell is enlarged to illustrate the geometric dimensions of the structure used in the simulation. The geometric dimensions are $a = 24$ μm, $b = 12$ μm, $t = 2$ μm, $r = 4$ μm, and $h = 50$ μm, respectively. (c) The transmission curve of the proposed metamaterials. The inset, which is used for comparison, exhibits the transmission curve for another metamaterials whose unit cell structure is one single metal plate the same as the bottom plate of the displayed metamaterials. The substrates supporting the metamaterials used in the numerical calculations are the same.

plates. The SRRs array erects on the polyimide substrate ($\varepsilon = 3.5 + 0.00945i$) with a thickness of 40 μm. Both the top and bottom aluminum plates (Al, $\sigma = 3.56 \times 10^7$ S/m) have a length of 24 μm, a width of 12 μm and a thickness of 2 μm. The lossy aluminum employed in the simulation is chosen from the material library of the simulation toolkit. The height and radius of the standing Al columns are 50 μm and 4 μm, respectively. The dimension of each unit cell is 100 μm $\times$ 100 μm. Fig. 1(c) demonstrates the calculated transmission curve of the metamaterials, which displays two resonance mode (Mode 1 and Mode 2) at 1.45 THz and 1.91 THz, respectively. All the numerical calculations are based on the finite integration method frequency domain solver. The *unit cell* boundary is used in the simulation to mimic the SRR array. The inset in Fig. 1(c) shows the calculated result of the transmission curve of a single Al plate the same as the bottom plate of the proposed metamaterials lying on the same polyimide substrate, which will be detailed in next subsection 2.2 and used for comparison to clarify the underlying physics of the Mode 2.

2.2 Analysis of Resonance Modes

To explore the physics behind the resonances of the three-dimensional metamaterials, the EM field distributions at the resonant frequencies are calculated. As shown in Fig. 2, the subfigures Fig. 2(a)–(c) in the first column demonstrate the resonance at 1.45 THz (Mode 1) is a fundamental LC resonance. The surface electric current on the SRR forms a half circle, as marked by the red arrow in Fig. 2(a). The out-of-phase electric fields [see Fig. 2(b)] shown at the edges of the top and bottom plates and strong magnetic dipole moment [see Fig. 2(c)] generated in the SRR have proven it sufficiently.

For Mode 2, the resonance mode is much more complicated. As shown in Fig. 2(d), the surface electric current on the bottom plate changes its direction compared to that shown in Fig. 2(a), while the other current directions remain the same. Also shown in Fig. 2(d), the surface current at Mode 2 distribute more uniformly instead of centering on the surface of the standing column displayed in Fig. 1(a), but with slightly more current centering on the bottom plate. This is induced by the higher refractive index environment near the substrate compared to the air around the top plate. The electric field on the top and bottom plates resonates in-phase, as displayed in Fig. 2(e). As a result, two magnetic moments with opposite directions come into being around the corners of the SRR, as shown in Fig. 2(f). To clarify the resonance attributes of Mode 2, additional simulations are conducted. First, a single Al plate with the same geometry as the bottom plate of the presented metamaterials lying on the same polyimide substrate under the same environmental condition described in Fig. 1(a) is numerically calculated and the result is shown in the inset of Fig. 1(c). The result illustrates that a resonant mode similar to Mode 2 is activated at 1.91 THz with a slightly lower resonant frequency and higher resonant amplitude, compared to Mode 2. Therefore, it can

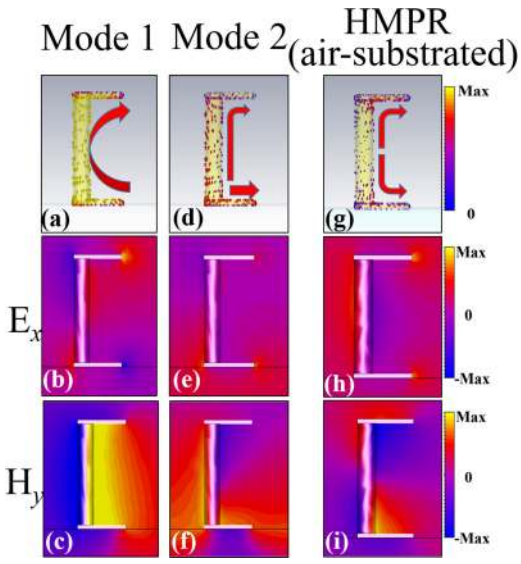

Fig. 2. (a), (b) and (c) display the surface electric current, electric and magnetic field intensity distributions, respectively, at Mode 1. (d), (e) and (f) demonstrate the surface electric current, electric and magnetic field intensity distributions, respectively, at Mode 2. All the electric and magnetic field intensity distributions are calculated at $y = 0$ of *xoz* plane. To further illustrate resonant property of Mode 2, the substrate materials of the proposed metamaterials is replaced with air. The subfigures, i.e., (g), (h) and (f), disclose the surface electric current, electric and magnetic field intensity distributions for the new air-substrated metamaterials at the corresponding resonance frequency. The thickness and direction of the red arrows in Fig. 2(a), (d), and (g) denote the distribution density and direction of the surface electric current.

be inferred that the bottom plate as well as the top one plays a significantly dominant role in the formation of Mode 2. Also, it is well-established that this resonance mode displayed in the inset of Fig. 1(c) can be regarded as an electric dipole resonance [17]. However, in our case, Mode 2 is not a simple electric dipole resonance due to the disturbance of the standing column. The metal column is able to guide the free charges to resonate back and forth along the SRRs driven by the electric and magnetic field components of the incident THz waves together, which develops a different resonant mechanism.

Next, we change the substrate material of the three-dimension SRR metamaterials into air with other configuration unaltered. The EM field intensity distributions of the new metamaterials at the corresponding resonant frequency are shown in Fig. 2(g)–(i). Compared with the relevant subfigures [see Fig. 2(d)–(f)] of Mode 2, we can notice the field distributions are similar but with some slight differences. As displayed in Fig. 2(g) and (i), the surface electric currents show mirror symmetry relative to the middle place of the column and as a result, two magnetic moments with opposite directions dividing apart from the same middle place show up. The replacement of polyimide substrate with air eliminates the influence of refractive index environment difference around the SRRs, which induces the symmetric distributions and also the observable exhibition of the physical meanings of Mode 2. According to the naming rule in [17], Mode 2 can be termed as HMPR mode.

2.3 Influences of Structural Geometries Tunings

In this subsection, the influences of the changing of the various geometric parameters of the metamaterials on the THz spectral response will be discussed. First, the influence of geometric parameters of the metal plates is discussed. As shown in Fig. 3(a) and (b), the resonant frequencies of Mode 1 and Mode 2 demonstrate continuous red-shift with the geometry of the metal plate

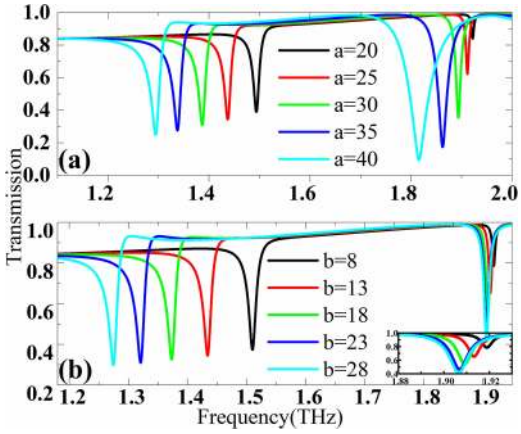

Fig. 3. The impact of the changing of the geometrical dimensions of the top and bottom plates on the transmission spectra. (a) The length *a* changes with the fixed $b = 12$ μm. (b) The width *b* changes with the fixed $a = 24$ μm. The inset in (b) shows the enlarged part of transmission curve near Mode 2.

enlarging resulting from the inherent scalability of metamaterials. The length and width of the metal plates display strong modulation for Mode 1, while for Mode 2, the modulation effect of the length is more obvious than that of the width, especially in term of the modulation of the resonant frequency location. The inset of Fig. 3(b) displays the details of the resonant amplitude and frequency variations of Mode 2.

Next, the impact of the dimensional alterations of the height of the standing column is analyzed. As displayed in Fig. 4(a), the resonant frequencies of Mode 1 redshift continuously with the height of the column increasing, which is similar to the tuning behaviors in cases of the geometric change of the metal plates. However, the height changes of the column show a rather weak impact on the resonant frequency and amplitude of Mode 2. To be specific, when the height *h* increases from 26 μm to 50 μm, the resonant frequencies show redshift but with a fairly small rate. The corresponding percentage variations in the absolute value for the resonant frequency are less than 0.5%, compared to 1.91 THz when $h = 50$ μm [see Fig. 1(c)]. Also, as shown in Fig. 4(a), the resonant amplitudes of Mode 2 demonstrates the similar phenomenon, i.e., the amplitude percentage variations in the absolute value are less than 6.5% when *h* equal to or larger than 26 μm, compared to the resonant amplitude of 0.6781 when $h = 50$ μm [see Fig. 1(c)]. In addition, as the height of the column enlarges, the quality factors (Q) of Mode 1 and Mode 2 change as well. The Q value is calculated as $Q = f_0/FWHM$, f_0 is the central frequency of the resonance and FWHM means full width at half maximum. As displayed in Fig. 4(b), the Q values for Mode 1 range from 77 to 89 while the Q values for Mode 2 increase from 259 to about 270. All these results indicate that the three-dimensional SRR metamaterials can produce dual-band magnetic plasmon resonances with high Q. Fig. 4(c) exhibits the frequency interval between the dual-band resonances changes from 0.15 THz to 0.47 THz as the height *h* increases from 26 μm to 50 μm. The frequency interval is the difference value between the central frequencies of the two resonances. The polynomial fitting equation for the changing trend is $\Delta f = -0.0002h^2 + 0.026h - 0.4086$ with the goodness of fit of $R^2 = 0.9999$. The goodness of fit (R^2) denotes the approximate extent that the fitting equation can describe the changing trend of fitted data. The closer R^2 is to 1, the better representative result the fitting equation shows. It is also worth noting that there is a geometric limitation for the height of the column to maintain the realization of HMPR. To explore this limitation, we also numerically calculate the changing trend of the transmission curves when decreasing the low height column of 30 μm with a step of 5 μm. When the height is equal to or above 25 μm, the evolution for both LC mode and HMPR is clearly stated in advance and drawn in Fig. 4(d) to compare with the cases of the height below 25 μm. As indicated by the purple dashed curve in Fig. 4(d), the resonance frequency of LC mode blueshifts gradually at first, however, becomes stable near 1.91 THz almost coinciding with

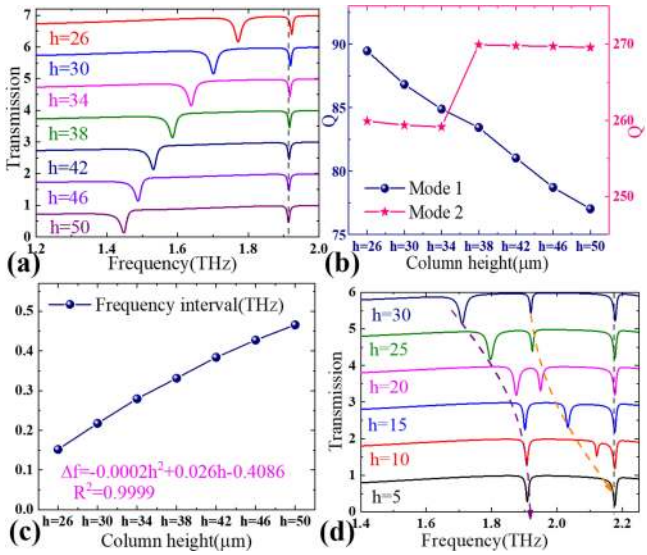

Fig. 4. (a) Transmission curve evolution with the height increasing from $h = 26$ μm to $h = 50$ μm and the other geometric parameters identical to those shown in caption of Fig. 1. The vertical dashed lines show the deviations of all the curves from the resonant frequency of 1.91 THz. (b) The Q value variations for Mode 1 and Mode 2 with the height changing. (c) The frequency interval changing trend with the alteration of the height and also the relevant polynomial fitting equation and the goodness of fit (R^2) for the trend. (d) To discuss the limitation of the influence of the height on the resonances evolution and coupling effect between top and bottom plates, the changing trend of the transmission spectra decreasing the low height with a step of 5 μm is calculated and shown. The purple and orange dashed curves are used to guide eyes to track the resonance frequency shifts of LC resonance and HMPR, respectively. The resonance at 2.17 THz is a pure electric resonance produced by the bottom aluminum plate, as marked by a vertical black dashed line.

that of HMPR. Similarly, the resonance location of HMPR shifts towards high frequency with the amplitude diminishing during the process. Eventually, HMPR totally degenerates into the resonance at 2.17 THz which is a pure electric resonance uncovered by the surface electric current distribution (not shown here). The resonance at 2.17 THz is induced solely by the electric currents resonating on the bottom plate and can also be proved by the constant resonance frequency location with the alterations of the height. To understand these interesting evolutionary phenomena, we calculate the electric and magnetic field and surface electric current distributions at the corresponding resonance frequencies for the different cases displayed in Fig. 4(d). We note that when the height is compressed below 25 μm or less, the division between two magnetic moments with opposite directions for HMPR becomes increasingly vague at first, changes into a weak modified LC resonance in the middle process and finally weakens continuingly into a pure electric resonance. These findings unmask that HMPR of the three-dimension SRR metamaterials requires enough high supporting column to support its specific EM field distribution and in our case, the critical height of column is 25 μm.

Finally, Fig. 5 presents the variation trend for both the resonance modes with the column radius of the metamaterials changing. As displayed in Fig. 5(a), Mode 1 demonstrates continuous blue-shift as the column thickens while Mode 2 reveals rather weak dependence on the radius alterations. When the radius increases from $r = 1$ μm to $r = 8$ μm, the resonant frequencies percentage variations in the absolute value are less than 0.13% compared to 1.91 THz when $r = 4$ μm while the resonance amplitude percentages are less than 7.54%, compared to 0.6781 when $r = 4$ μm. All these insignificant numbers substantiate the independent relationship between Mode 2 and the radius of the column. As displayed in Fig. 5(b), the Q values increase monotonously from 37 to 176 for Mode 1, but vary smoothly from 266 to 270 for Mode 2. The frequency interval for the two modes decreases monotonously from 0.78 THz to 0.21 THz with the radius enlarging. The fitting

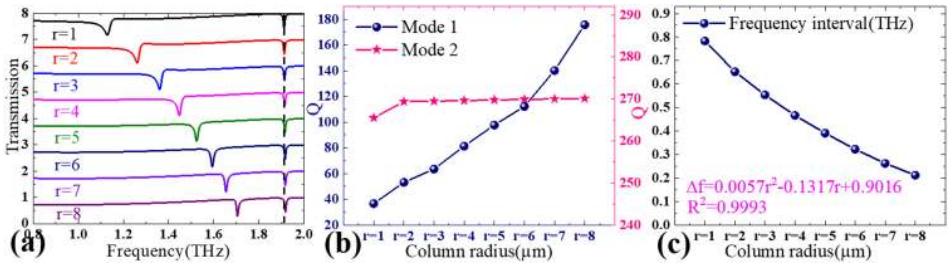

Fig. 5. (a) Transmission curve evolution with the radius increasing from $r = 1$ μm to $r = 8$ μm and the other geometric parameters identical to those shown in caption of Fig. 1. The vertical dashed lines show the deviations of all the curves from the resonant frequency of 1.91 THz. (b) The Q value variation for Mode 1 and Mode 2 as the radius changes. (c) The frequency interval changing trend for the alteration of the radius and the resulted fitting equation and the goodness of fit for the trend.

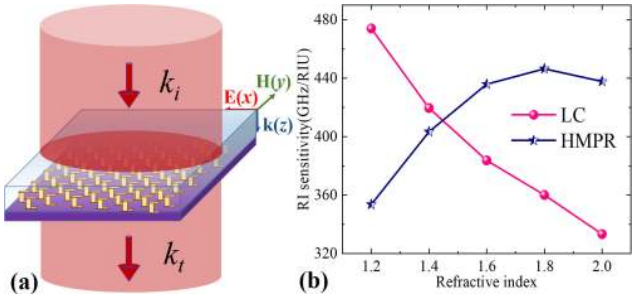

Fig. 6. (a) Schematic drawing of sensing configuration based on our proposed three-dimensional metamaterials. An analyte to be tested with a thickness of 70 μm is added onto the top surface of the metamaterial sensor. (b) The change of refractive index (RI) sensitivity versus RI alteration for LC mode and HMPR, respectively.

equation is also shown in Fig. 5(c), $\Delta f = 0.0057r^2 - 0.1317r + 0.9016$ with a goodness of fit of $R^2 = 0.9993$.

The weak dependent relationship between Mode 2 and the geometric dimensions of the column can be explained by the resonant characteristic of Mode 2 shown in Fig. 2. The top and bottom metal plates play crucial role in the formation of Mode 2 while the column just guides the electric currents to oscillate along the SRRs. Therefore, when the geometric dimensions of the plates are fixed, the resonant frequency location and amplitude are almost determined accordingly. As a result, the variations in the column show a weak impact on the spectral response. In this case, it is convenient to design magnetic metamaterials with the dual-band, even multi-band, magnetic plasmon resonance modes with customized frequency interval.

3. Further Discussion

In this section, first, we evaluate refractive index (RI) sensing performance of our presented metamaterials in terms of the application prospective. Benefiting from vertical configuration of this kind of three-dimensional metamaterials, the sensing performance will be enhanced largely [31]. The sensing performance evaluation for gaseous or liquid substance is conducted here to maximize the calculated sensitivity, since the substance is able to contact the sensor adequately when the substance is gaseous or liquid. As shown in Fig. 6(a), an analyte with a thickness of 70 μm is placed onto the metamaterial sensor to implement the sensing procedure. This selected thickness is so large that it can avoid the influence of thickness in the process of the RI sensing [31]. Then we change RI of the analyte from 1.2 to 2 with a step of 0.2. The frequency locations of LC mode and HMPR demonstrate continuous red-shifts with the increase of RI. The RI sensitivity is calculated by

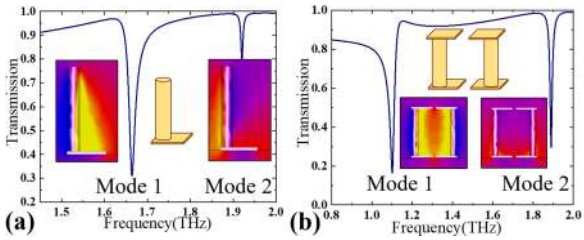

Fig. 7. (a) The similar resonant modes are demonstrated in standing L-shaped metamaterials. The middle inset demonstrate the unit cell structure. The left and right insets demonstrate the magnetic field density distributions for two modes, respectively. (b) The similar resonant modes are displayed in symmetric standing SRR metamaterials. The upper inset displays the unit cell design. The left and right insets show the respective magnetic field density distributions.

$S = (f_0 - f)/\Delta n$, the S denotes the RI sensitivity and the f is the resonance frequency location of the metamaterials coated by an analyte while the f_0 is the central frequency of the metamaterial sensor with no analyte. The Δn is the RI difference inducing the shift of the central frequency of resonances. From Fig. 6(b), the RI sensitivity monotonously decreases from 474 GHz/ RIU to 333 GHz/ RIU for LC mode, while an opposite trend for HMPR appears, that is RI sensitivity increasing gradually from 354 GHz/ RIU and approaching the maximum of about 446 GHz/ RIU for higher RI. Although the RI sensitivity of the three-dimensional metamaterials is not so well as that displayed in [31], it still promises a good metamaterial sensor compared with planar metamaterial sensors [43].

We further probe the existence of the HMPR mode in other similar metamaterial design. As shown in Fig. 7(a), similar resonance modes arise in the standing L-shaped three-dimension SRR metamaterials. The inset in Fig. 7(a) displays the unit cell structure of the L-shaped three-dimension SRR metamaterials. The central frequency of Mode 2 is 1.92 THz which is close to that shown in Fig. 1(c). The additional numerical results for the EM field density distributions also displayed in Fig. 7(a) prove that Mode 1 at 1.66 THz is still a fundamental LC resonance and Mode 2 remains the HMPR. Fig. 7(b) displays the unit cell structure of the symmetric three-dimension SRR metamaterial and the transmission curve. The EM field density distributions displayed in Fig. 7(b) indicate Mode 1 at 1.10 THz is the LC resonance mode and Mode 2 at 1.89 THz is the HMPR as well. Based on above discussions, we notice that when the geometric dimensions of constituent top (or/and bottom) plates of that kind of three-dimension SRR metamaterials are fixed, HMPR will be always activated near the constant resonant frequency with different resonant amplitudes. Furthermore, the tuning behaviors of the geometric dimensions of these three-dimension metamaterials are numerically analyzed as well. The calculated results (not shown in the paper) illustrate the same tuning characteristics, i.e., Mode 2 shows little dependence on the columns of metamaterials.

4. Conclusion

In summary, we exhibit a type of three-dimension SRR metamaterials with dual-band magnetic resonances in the paper. The simulations reveal the two resonance modes are LC mode and high-order magnetic resonance mode, respectively. By analyzing the influences of geometric parameters of the metamaterials on the dual resonance modes, we observe that when the dimensions of the constituent top/bottom plates of the metamaterials are constant, only the LC resonance can be manipulated by tuning the dimensions of the column of the metamaterials since the HMPR mode demonstrates independence on the dimensions of the column. Therefore, we can design magnetic metamaterials with the dual-band or multi-band, magnetic plasmon resonance with customized frequency interval by simply designing the geometric parameters of this kind of the metamaterials. The sensing performance evaluation also suggests a good sensing prospective of our designed metamaterials. Our work contributes to the design of the multi-band magnetic metamaterials and will be helpful for other more complicated applications, like sensing and medical imaging techniques.

References

[1] S. Tan *et al.*, "Terahertz metasurfaces with a high refractive index enhanced by the strong nearest neighbor coupling," *Opt. Exp.*, vol. 23, no. 22, pp. 29222–29230, 2015.
[2] J. B. Pendry, "Negative refraction makes a perfect lens," *Phys. Rev. Lett.*, vol. 85, no. 18, pp. 3966–3969, 2000.
[3] R. A. Shelby, D. R. Smith, and S. Schultz, "Experimental verification of a negative index of refraction," *Science*, vol. 292, no. 5514, pp. 77–79, 2001.
[4] V. G. Veselago, "The electrodynamics of substances with simultaneously negative values of ε and μ," *Soviet Phys. Uspekhi*, vol. 10, no. 4, pp. 509–514, 1968.
[5] N. I. Landy, S. Sajuyigbe, J. J. Mock, D. R. Smith, and W. J. Padilla, "Perfect metamaterial absorber," *Phys. Rev. Lett.*, vol. 100, no. 20, 2008, Art. no. 207402.
[6] L. Ding, Q. Y. S. Wu, and J. H. Teng, "Polarization independent broadband terahertz antireflection by deep-subwavelength thin metallic mesh," *Laser Photon. Rev.*, vol. 8, no. 6, pp. 941–945, 2015.
[7] S. Zhang, D. A. Genov, Y. Wang, M. Liu, and X. Zhang, "Plasmon-induced transparency in metamaterials," *Phys. Rev. Lett.*, vol. 101, no. 4, 2008, Art. no. 047401.
[8] N. K. Grady *et al.*, "Terahertz metamaterials for linear polarization conversion and anomalous refraction," *Science*, vol. 340, no. 6138, pp. 1304–1307, 2013.
[9] J. Xiang *et al.*, "Polarization beam splitters, converters and analyzers based on a metasurface composed of regularly arranged silicon nanospheres with controllable coupling strength," *Opt. Exp.*, vol. 24, no. 11, pp. 11420–11434, 2016.
[10] F. Ding, R. Deshpande, and S. I. Bozhevolnyi, "Bifunctional gap-plasmon metasurfaces for visible light: Polarization-controlled unidirectional surface plasmon excitation and beam steering at normal incidence," *Light, Sci. Appl.*, vol. 7, 2018, Art. no. 17178.
[11] J. B. Pendry, A. J. Holden, W. J. Stewart, and I. I. Youngs, "Extremely low frequency plasmons in metallic mesostructures," *Phys. Rev. Lett.*, vol. 76, no. 25, pp. 4773–4776, 1996.
[12] J. B. Pendry, A. J. Holden, D. J. Robbins, and W. J. Stewart, "Magnetism from conductors and enhanced nonlinear phenomena," *IEEE Trans. Microw. Theory Techn.*, vol. 47, no. 11, pp. 2075–2084, Nov. 1999.
[13] D. Schurig, J. J. Mock, and D. R. Smith, "Electric-field-coupled resonators for negative permittivity metamaterials," *Appl. Phys. Lett.*, vol. 88, no. 4, 2006, Art. no. 041109.
[14] V. A. Fedotov, M. Rose, S. L. Prosvirnin, N. Papasimakis, and N. I. Zheludev, "Sharp trapped-mode resonances in planar metamaterials with a broken structural symmetry," *Phys. Rev. Lett.*, vol. 99, no. 14, 2007, Art. no. 147401.
[15] T. Kaelberer, V. A. Fedotov, N. Papasimakis, D. P. Tsai, and N. I. Zheludev, "Toroidal dipolar response in a metamaterial," *Science*, vol. 330, no. 6010, pp. 1510–1512, 2010.
[16] M. Manjappa, S. P. Turaga, Y. K. Srivastava, A. A. Bettiol, and R. Singh, "Magnetic annihilation of the dark mode in a strongly coupled bright-dark terahertz metamaterial," *Opt. Lett.*, vol. 42, no. 11, pp. 2106–2109, 2017.
[17] C. Rockstuhl, F. Lederer, C. Etrich, T. Zentgraf, J. Kuhl, and H. Giessen, "On the reinterpretation of resonances in split-ring-resonators at normal incidence," *Opt. Exp.*, vol. 14, no. 19, pp. 8827–8836, 2006.
[18] S. Linden, C. Enkrich, M. Wegener, J. Zhou, T. Koschny, and C. M. Soukoulis, "Magnetic response of metamaterials at 100 terahertz," *Science*, vol. 306, no. 5700, pp. 1351–1353, 2004.
[19] D. B. Burckel *et al.*, "Micrometer-scale cubic unit cell 3D metamaterial layers," *Adv. Mater.*, vol. 22, no. 44, pp. 5053–5057, 2010.
[20] C. C. Chen *et al.*, "Fabrication of three dimensional split ring resonators by stress-driven assembly method," *Opt. Exp.*, vol. 20, no. 9, pp. 9415–9420, 2012.
[21] W. T. Chen *et al.*, "Optical magnetic response in three-dimensional metamaterial of upright plasmonic meta-molecules," *Opt. Exp.*, vol. 19, no. 13, pp. 12837–12842, 2011.
[22] K. Fan, A. C. Strikwerda, H. Tao, X. Zhang, and R. D. Averitt, "Stand-up magnetic metamaterials at terahertz frequencies," *Opt. Exp.*, vol. 19, no. 13, pp. 12619–12627, 2011.
[23] K. Fan, A. C. Strikwerda, X. Zhang, and R. D. Averitt, "Three dimensional broadband tunable terahertz metamaterials," *Phys. Rev. B, Condens. Matter*, vol. 87, no. 16, 2013, Art. no. 161104.
[24] W.-L. Hsu *et al.*, "Vertical split-ring resonator based anomalous beam steering with high extinction ratio," *Sci. Rep.*, vol. 5, 2015, Art. no. 11226.
[25] D. Liang *et al.*, "Plasmonic analog of electromagnetically induced transparency in stereo metamaterials," *IEEE J. Sel. Topics Quantum Electron.*, vol. 23, no. 4, Jul./Aug. 2017, Art. no. 4700907.
[26] P. C. Wu *et al.*, "Magnetic plasmon induced transparency in three-dimensional metamolecules," *Nanophotonics*, vol. 1, no. 2, pp. 131–138, 2012.
[27] Z. Liu *et al.*, "High-quality-factor mid-infrared toroidal excitation in folded 3d metamaterials," *Adv. Mater.*, vol. 29, 2017, Art. no. pp. 1606298.
[28] P. C. Wu *et al.*, "Plasmon coupling in vertical split-ring resonator metamolecules," *Sci. Rep.*, vol. 5, 2015, Art. no. 9726.
[29] P. C. Wu *et al.*, "Vertical split-ring resonator based nanoplasmonic sensor," *Appl. Phys. Lett.*, vol. 105, no. 3, 2014, Art. no. 033105.
[30] P. C. Wu, C. Y. Liao, J. W. Chen, and D. P. Tsai, "Isotropic absorption and sensor of vertical split-ring resonator, " *Adv. Opt. Mater.*, vol. 5, no. 2, 2017, Art. no. 1600581.
[31] W. Wang, F. Yan, S. Tan, H. Zhou, and Y. Hou, "Ultrasensitive terahertz metamaterial sensor based on vertical split ring resonators," *Photon. Res.*, vol. 5, no. 6, pp. 571–577, 2017.
[32] S. Liu, J. Du, Z. Lin, R. X. Wu, and S. T. Chui, "Formation of robust and completely tunable resonant photonic band gaps," *Phys. Rev. B*, vol. 78, no. 15, 2008, Art. no. 155101.
[33] S. Liu, W. Chen, J. Du, Z. Lin, S. T. Chui, and C. T. Chan, "Manipulating negative-refractive behavior with a magnetic field," *Phys. Rev. Lett.*, vol. 101, no. 15, 2008, Art. no. 157407.
[34] H. Wu, Q. Luo, H. Chen, Y. Han, X. Yu, and S. Liu, "Magnetically controllable nonreciprocal Goos-Hänchen shift supported by a magnetic plasmonic gradient metasurface," *Phys. Rev. A*, vol. 99, no. 3, 2019, Art. no. 033820.

[35] M. W. Klein, C. Enkrich, M. Wegener, and S. Linden, "Second-harmonic generation from magnetic metamaterials," *Science*, vol. 313, no. 5786, pp. 502–504, 2006.
[36] M. Lapine, I. V. Shadrivov, D. A. Powell, and Y. S. Kivshar, "Magnetoelastic metamaterials," *Nature Mater.*, vol. 11, pp. 30–33, 2011.
[37] H. Liu *et al.*, "Magnetic plasmon hybridization and optical activity at optical frequencies in metallic nanostructures," *Phys. Rev. B*, vol. 76, no. 7, 2007, Art. no. 073101.
[38] N. Liu *et al.*, "Magnetic plasmon formation and propagation in artificial aromatic molecules," *Nano Lett.*, vol. 12, no. 1, pp. 364–369, 2012.
[39] H. Chen *et al.*, "Manipulating unidirectional edge states via magnetic plasmonic gradient metasurfaces," *Plasmonics*, vol. 12, no. 4, pp. 1079–1090, Aug. 2017.
[40] S. Liu, W. Lu, Z. Lin, and S. T. Chui, "Molding reflection from metamaterials based on magnetic surface plasmons," *Phys. Rev. B*, vol. 84, no. 4, 2011, Art. no. 045425.
[41] J. Yu, H. Chen, Y. Wu, and S. Liu, "Magnetically manipulable perfect unidirectional absorber based on nonreciprocal magnetic surface plasmon," *Europhys. Lett.*, vol. 100, no. 4, 2012, Art. no. 47007.
[42] R. Schmidt and A. Webb, "Metamaterial combining electric- and magnetic-dipole-based configurations for unique dual-band signal enhancement in ultrahigh-field magnetic resonance imaging," *ACS Appl. Mater. Interfaces*, vol. 9, no. 40, pp. 34618–34624, 2017.
[43] I. Al-Naib, "Biomedical sensing with conductively coupled terahertz metamaterial resonators," *IEEE J. Sel. Topics Quantum Electron.*, vol. 23, no. 4, Jul./Aug. 2017, Art. no. 4700405.